Chemistry–A European Journal

Research Article
doi.org/10.1002/chem.202202629

Chemistry Europe
European Chemical Societies Publishing

www.chemeurj.org

N_2 Reduction versus H_2 Evolution in a Molybdenum- or Tungsten-Based Small-Molecule Model System of Nitrogenase

Jannik Junge,[a] Tobias A. Engesser,[a] and Felix Tuczek*[a]

Abstract: Molybdenum dinitrogen complexes have played a major role as catalytic model systems of nitrogenase. In comparison, analogous tungsten complexes have in most cases found to be catalytically inactive. Herein, a tungsten complex was shown to be supported by a pentadentate tetrapodal (pentaPod) phosphine ligand, under conditions of N_2 fixation, primarily catalyzes the hydrogen evolution reaction (HER), in contrast to its Mo analogue, which catalytically mediates the nitrogen-reduction reaction (N_2RR). DFT calculations were employed to evaluate possible mechanisms and identify the most likely pathways of N_2RR and HER activities exhibited by Mo- and W-pentaPod complexes. Two mechanisms for N_2RR by PCET are considered, starting from neutral (M(0) cycle) and cationic (M(I) cycle) dinitrogen complexes (M = Mo, W). The latter was found to be energetically more favorable. For HER three scenarios are treated; that is, through bimolecular reactions of early M-N_xH_y intermediates, pure hydride intermediates or mixed M(H)(N_xH_y) species.

Introduction

The catalytic conversion of dinitrogen to ammonia with transition metal complexes has been subject of research for many years.[1,2,3] Recently great progress has been made in terms of turnover numbers and efficiency.[3,4,5,6] A large part of synthetic nitrogen fixation has been devoted to molybdenum systems catalytically mediating the nitrogen reduction reaction (N_2RR).[2,6,7] In almost all known cases, analogous tungsten complexes have been found to be catalytically inactive.[8–10] Notably, the reason for this finding has hardly been investigated. Schrock and coworkers postulated for their triamidoamine system that the reason might lie in the difficult regeneration of the W(N_2) complex from the $[W(NH_3)]^+$ intermediate. This in turn may be due to more negative reduction potentials for tungsten complexes compared to their molybdenum analogues, which could be demonstrated for the W(N_2) to $[W(N_2)]^-$ step although this stage plays no role in the catalytic cycle. Additionally, no difference in redox potentials was observed for the M(0)↔M(I) transition.[8,11] On the other hand, tungsten oxo complexes have more negative redox potentials for the M(IV)↔M(V) transition than their molybdenum counterparts.[12] Whereas this redox transition is part of the catalytic cycle for the Schrock system (+III to +VI), it is not contained in the catalytic cycle of Chatt-type complexes (0 to +IV). Nevertheless, it suggests that the redox potentials for tungsten intermediates at higher oxidation states may indeed be more negative than for the molybdenum analogues.

Recently, we presented the first tungsten complex generating overstoichiometric amounts of ammonia (2.8 equiv) under (chemo-)catalytic conditions with SmI_2 and water.[10] Nevertheless, the tungsten complex is significantly less active than its molybdenum analogue (25.7 equiv).[5] Both of these complexes are supported by a pentadentate tetrapodal phosphine ligand ($P^{Me}{}_2PP^{Ph}{}_2$, pentaPod)[13] (Scheme 1).[14]

By cyclovoltammetry we showed that the two complexes [M(N_2)(pentaPod)] (M = Mo (**1**) and W (**2**)) exhibit the same reduction potential for the M(0)↔M(I) transition.[10] Moreover, we could exclude a difference in the activation of the N_2 ligand and structural differences between these complexes as possible origins of the different activity towards N_2RR. The reason must therefore lie elsewhere in the catalytic cycle. We could observe a difference in stability of the $[M(I)\text{-}N_2]^+$ complexes where the

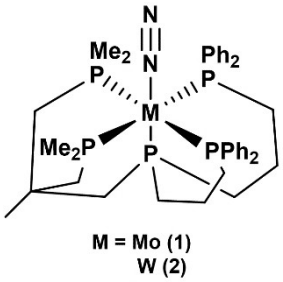

Scheme 1. Molybdenum and tungsten dinitrogen complex [M(N_2)($P^{Me}{}_2PP^{Ph}{}_2$)] (M = Mo (1) and W (2)) supported by a pentadentate tetrapodale phosphine ligand.

[a] *J. Junge, Dr. T. A. Engesser, Prof. Dr. F. Tuczek*
Institut für Anorganische Chemie
Christian-Albrechts-Universität zu Kiel
Max-Eyth-Strasse 2, 24118 Kiel (Germany)
E-mail: ftuczek@ac.uni-kiel.de

Supporting information for this article is available on the WWW under https://doi.org/10.1002/chem.202202629

dinitrogen ligand decoordinates in the molybdenum complex whereas it remains bound in the tungsten analogue.[10] However, the way in which this affects the catalytic activity remained unclear.

Hydrogen evolution is frequently encountered as a side-reaction in nitrogen-fixing systems. This also applies to nitrogenase where, however, it is an integral part of biological N_2-to-NH_3 conversion.[15] Synthetic nitrogen fixation, on the other hand, aims at totally suppressing HER in order to maximize the yield of ammonia.[16,17] Most N_2RR catalysts, however, do also mediate HER to some extent, and therefore it is important to understand and control the factors which influence the interplay between HER and N_2RR. Peters and coworkers showed that iron hydride species, which are partly generated during catalysis, can effectively produce hydrogen in a HER cycle parallel to the desired N_2RR cycle.[16,18] They also discovered that iron complexes supported by Al- and Ga-based ligand systems, which are more robust under catalytic conditions, seem to show more selectivity towards HER than to N_2RR[19] and that M–NNH species with a low N–H bond dissociation free energy (BDFE) can have a negative effect on the N_2RR efficiency, due to bimolecular HER.[16,20] On the other hand, Benedek et al. theoretically investigated the HER activity of early N_2RR intermediates in Peters' systems and came to the conclusion that early N_2RR intermediates are not likely the source of HER under catalytic conditions because the barriers of the competing N_2RR steps are significantly lower. They also considered the lifetime of these early intermediates very short so that bimolecular HER should only play a minor role.[21,22]

Herein, we first experimentally investigate the HER activities of molybdenum and tungsten complexes supported by the pentaPod ligand (Scheme 1), complementing the earlier data on N_2RR catalysis obtained for these systems.[5,10] Then we present a computational study in order to determine possible pathways of N_2RR and HER in these systems and identify potential reasons for the different reactivities of the Mo and W complex. To this end, the mechanism of a catalytic conversion of dinitrogen to ammonia is treated by DFT and the Gibbs free activation energies of HER and N_2RR elementary steps are calculated for both **1** and **2**. As discussed previously,[5] the catalytic conversion of dinitrogen to ammonia based on [Mo-$(N_2)(P^{Me}{}_2PP^{Ph}{}_2)$] (**1**) can be achieved thermodynamically from a M(0)-N_2 and a $[Mo(I)\text{-}N_2]^+$ species with SmI_2 and water. A PCET process starting from $[Mo(I)\text{-}N_2]^+$ is a highly exergonic process, while starting from the M(0)-N_2 species is slightly endergonic. We therefore investigate which catalytic cycle overall is thermodynamically more favorable and how the system may switch from a pathway originating from a M(0)-N_2 complex to a reaction path involving a $[M(I)\text{-}N_2]^+$ intermediate. Finally, kinetic barriers are explicitly determined for HER by bimolecular reactions and based on mixed $M(H)(N_xH_y)$ species. The implications of the results with respect to the optimization of catalysts mediating N_2RR are discussed.

Computational Details

Geometry Optimization and Frequency Calculations

All computations were carried out using the ORCA 4.2.1 program package.[23] The properties of all studied structures were computed in the most stable spin state, which was determined through theoretical analysis. Geometry optimization and thermodynamic energy calculations were carried out with the PBE0 functional[24] and def2-TZVP[25–27] basis set. In addition, Grimme's dispersion correction[28,29] with Becke-Johnson damping (D3BJ) and the RIJCOSX density fitting approximation using the def2/J fitting basis set[30–33] were used for all calculations. Due to the good agreement of the calculated geometries compared to crystallographic data (see Table S1) of $[M(N_2)(P^{Me}{}_2PP^{Ph}{}_2)]$ (M = Mo, W) it is assumed that the computational methodology has sufficient accuracy for geometry optimizations. Local minima were confirmed when no imaginary frequency was found in harmonic vibrational frequency calculations. For the complete theoretical data, see the Supporting Information Table S3 to S21.

Relativistic corrections could not be taken into account in the full pentaPod system due to the size of the system and the long computing time associated with it. Since relativistic effects should not be neglected, especially in the case of tungsten, the extent to which relativistic effects influence the energetics was determined. For this purpose, test calculations were carried out with smaller molybdenum and tungsten systems of the type $M(PMe_3)_5(L)$ (M = Mo, W; L = N_2, NNH, NNH_2) and the energetics of the first steps of a catalytic conversion were compared for different density functionals as well as using the zeroth order regular approximation (ZORA)[34] as relativistic correction (Table 1). When ZORA was used, the respective ZORA basis sets were applied.[35] Due to convergence problems additionally the KDIIS approximation was used.[36] Since there is no significant difference when using ZORA as relativistic correction, especially for the PBE0 density functional, it can be assumed that the effect is negligible in terms of Free Gibbs energy calculations.

Table 1. Comparison of calculated free Gibbs Energies of PCET reactions to the first two intermediates of the N_2RR with different density functionals and basis sets with and without relativistic corrections in kcal/mol. These calculations were made for neutral $[M(PMe_3)_5(L)]$ complexes (M = Mo, W; L = NNH, NNH_2).

functional	basis set	metal	PCET to [M(I)-NNH]	PCET to [M(II)-NNH_2]
BP86	def2-SVP	Mo	3.58	−22.12
		W	1.94	−22.25
	ZORA-def2-SVP	Mo	3.30	−23.68
		W	1.89	−24.33
PBE0	def2-TZVP	Mo	8.21	−19.20
		W	6.09	−19.50
	ZORA-def2-TZVP	Mo	9.03	−19.34
		W	6.35	−19.48

Table 2. Comparison of the activation barriers calculated with different density functionals and basis sets with and without relativistic corrections of the HER based on the Mo(II)(NNH)(H) complex.

density functional	BP86			PBE0		
basis set	def2-SVP	def2-TZVP	ZORA-def2-SVP	def2-SVP	def2-TZVP	ZORA-def2-TZVP
$\Delta G^{\ddagger}$ (kcal/mol)	6.18	6.60	7.24	11.49	11.68	12.82

Table 3. Influence of different density functionals and basis sets as well as relativistic corrections on the calculated $BDFE_{N-H}$ for the first two intermediates of the N_2RR cycle.

functional	basis set	metal	$BDFE_{N-H}$ [**M**(I)-NNH]	$BDFE_{N-H}$ [**M**(II)-NNH_2]
BP86	def2-SVP	Mo	22.4	48.1
		W	24.1	48.3
	ZORA-def2-SVP	Mo	22.7	49.7
		W	24.1	50.3
PBE0	def2-TZVP	Mo	17.8	45.2
		W	19.9	45.5
	ZORA-def2-TZVP	Mo	17.0	45.3
		W	19.7	45.5

M = $M(PMe_3)_5$.

Calculation of Activation Barriers

For calculations of activation Gibbs free energies of the HER we located the first order saddle points on the potential energy hypersurface which correspond to the transition states of the reaction. The presence of one imaginary frequency in vibrational spectrum, belonging to the formation of a hydrogen molecule, confirmed the transition state. Therefore, we resorted to the BP86 functional[37] with the def2-SVP[25–27] basis set to reduce computational time. An exemplary comparison of the calculations with the BP86 density functional compared to the PBE0 density functional based on the transition state of the Mo(II)(H)(NNH) species shows a difference of approx. 5 kcal/mol, which is sufficient accuracy for a comparison of the most probable paths for the HER (Table 2). Notably, the BP86 density functional seems to underestimate the activation barrier compared to the PBE0 density functional. In addition, calculations in which relativistic corrections with ZORA were performed, which only show a difference of 1 kcal/mol for molybdenum (see Table 2). Due to the small difference when considering relativistic corrections for molybdenum, this correction was not used in the calculations, as it increased the calculation time considerably. For tungsten, such calculations could not be achieved due to the long computing time when using the respective ZORA basis sets for the tungsten atom.

For monomolecular HER, the ground state of the initial state is always found to coincide with that of the product. This is not the case for bimolecular HER, where both spin-allowed and spin-forbidden pathways are feasible in the reactions studied.[38] While the former can be treated with traditional spin-state theory, for the latter the crossing points of the minimum energy between the potential energy surfaces of the involved spin states have to be found.[39] Due to the large computational cost for large systems such as those studied here, we approximated the barriers by determining the transition states in all possible spin states and taking the Gibbs free energy of the transition state with the lowest energy.

Calculation of Single Point Energies

Single Point energies were determined with the PBE0 functional[24] and a def2-QZVPP[27] basis set. Solvation corrections were performed in THF solution using the solvation model based on density (SMD).[40] The solvation free energy ΔG_{solv} was approximated using the gas-phase and solvated single-point energies ($\Delta G_{solv} \approx E_{soln} - E_{gas}$).[16] In addition, Grimme's dispersion correction[28,29] with Becke-Johnson damping (D3BJ) and the RIJCOSX density fitting approximation using the def2/J fitting basis set[30–33] were used.

Calculation of PCET Reactions and Bond Dissociation Free Enthalpies (BDFEs)

Free reaction enthalpies of PCET reactions, ΔG(PCET), were theoretically calculated with TEMPO-H (TEMPO = 2,2,6,6-tetramethylpiperidine-1-yl)oxyl) as PCET reagent; i.e., for the reaction

$$\text{M-N}_x\text{H}_y + \text{TEMPO-H} \longrightarrow \text{M-N}_x\text{H}_{y+1} + \text{TEMPO}^{\cdot}$$

TEMPO-H has an experimentally determined $BDFE_{O-H}$ of 65.5 kcal/mol in THF.[41] Since in our experiments a mixture of SmI_2 and water is used as PCET reagent, which has a $BDFE_{O-H}$ of 26 kcal/mol,[42] the difference is added to ΔG(PCET) in order to obtain the Gibbs free energy for the PCET reaction of an M-N_xH_y intermediate with SmI_2/H_2O:

$$\Delta G_R(SmI_2/H_2O) = \Delta G(\text{PCET}) - (65.5\ \text{kcal/mol} - 26.0\ \text{kcal/mol})$$

N–H bond dissociation free enthalpies, $BDFE_{N-H}$, of the M-N_xH_y intermediates were also calculated based on the reaction with TEMPO-H as reference; i.e.

$$BDFE_{N-H}(\text{M-N}_x\text{H}_y) = 65.5\ \text{kcal/mol} - \Delta G(\text{PCET})$$

To validate this methodology we calculated the $BDFE_{N-H}$ for the $P_3{}^BFe(NNH)$ system ($P_3{}^B$ = tris(phosphine)borane) and compared it with values obtained by Peters and coworkers[16] and Benedek et al.,[21] respectively, showing close agreement (see Table S2).

In addition, we investigated the impact of relativistic effects on the BDFE's for our system exemplarily for the first intermediates of the M(0) cycle based on the employed density functionals and basis sets (Table 3). The result was a negligible influence of relativistics, while variation of the density functional-basis set combination caused differences of 5 kcal/mol.

Results and Discussion

In order to analyze the HER activity of the molybdenum and tungsten dinitrogen complexes [Mo(N_2)($P^{Me}_2PP^{Ph}_2$)] (**1**) and [W(N_2)($P^{Me}_2PP^{Ph}_2$)] (**2**) under catalytic conditions with SmI_2 and water the amount of hydrogen after a catalytic run was investigated by gas chromatographic analysis of the headspace (for details see Supporting Information). For the Mo-complex **1** 52.0 equiv (58% yield based on the reducing agent) of hydrogen could be detected together with 25.7 equiv[5] of ammonia (42%). In contrast, for the W-analogue **2** 79.7 equiv (89%) of hydrogen was detected, while only 2.8 equiv ammonia (5%) was found, showing that almost all of the reductant is used for HER at the tungsten complex and only a small amount for ammonia generation (see Figure 1 and Table 4). Background HER was neglected, as it was shown that the amount does not represent more than 2%.[6] Nishibayashi et al. observed the formation of small amounts of hydrazine in a W-based system, which they explained with protonation of the, compared to its molybdenum analogue, more electron-rich tungsten center of the hydrazido intermediate (W=N–NH_2).[9]

Notably, no hydrazine was found for our tungsten complex **2** under catalytic conditions. However, the explanation might give a clue regarding the reactivity differences between Mo and W complexes, since protonation and PCET reaction on the tungsten center could lead to hydrido complexes and thus could be responsible for the increased HER activity of tungsten complexes compared to their molybdenum analogues.

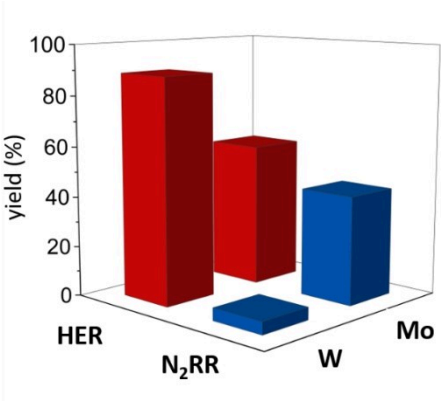

Figure 1. Yields (%) of ammonia (blue, N_2RR) and hydrogen (red, HER) obtained with the tungsten (**W**) and molybdenum (**Mo**) dinitrogen complex **1** and **2**, respectively, after catalytic runs with N_2 and SmI_2/water (cf Table 4).

N_2RR Pathways

To investigate the different pathways for hydrogen evolution under catalytic conditions it is necessary to determine the mechanism of catalytic N_2-to-NH_3 conversion at first. As discussed in our recent work,[5] the first PCET step of the catalytic cycle leading to the diazenido(−) (NNH^-) intermediate is energetically possible starting from a M(0)- as well as from a M(I)- dinitrogen complex. However, this step is slightly endergonic for the M(0) complex whereas it is exergonic for its M(I) counterpart.[5] A relevant question therefore is how to switch to a catalytic cycle based on a $[M(I)\text{-}N_2]^+$ complex if a M(0)-N_2 complex is employed as catalyst. Moreover, it is necessary to investigate which pathway is more feasible when the complete catalytic cycle is considered. To obtain information on this point, DFT calculations are conducted for both cases. In addition, the two cycles are also computed for the tungsten complexes for comparison with the molybdenum analogues, and possible reaction pathways for the transition from the M(0) cycle to the M(I) cycle are identified (see the Supporting Information).

The general mechanism of the two cycles is similar, but the intermediates differ in their oxidation state and charge. While in the M(0) cycle the invariably neutral intermediates undergo metal oxidation states between 0 and +III, the intermediates in the M(I) cycle, which are all mono-cationic complexes, assume metal oxidation states between +I and +IV (Figure 2). As already mentioned, the first step (PCET reaction to the M-NNH species) corresponds to an endergonic reaction in the M(0) cycle with +8.7 kcal/mol for molybdenum and +6.4 kcal/mol for tungsten while this reaction is strongly exergonic when starting from a $[M(I)\text{-}N_2]^+$ complex (−19.8 kcal/mol for Mo and −23.6 kcal/mol for W). The reaction to the M-NNH_2 intermediates is exergonic in both cases, showing slightly more negative values for the M(0) cycle. The next step to the Mo-NNH_3 intermediate is almost energy-neutral for both cycles with slightly endergonic values (+0.5 kcal/mol for Mo and W) for the M(0) cycle and slightly exergonic values (−1.1 kcal/mol for Mo and −1.6 kcal/mol for W) for the M(I) cycle. N–N splitting and release of one molecule ammonia under formation of a nitride species is the most exergonic reaction for both pathways with approx. −50 kcal/mol in the M(0) cycle and about −65 kcal/mol in the M(I) cycle for both metal centers. The following reaction steps show more negative values for the M(0) cycle compared to the M(I) cycle but are all strongly exergonic. Comparison of both cycles show that the M(I) cycle should be energetically more feasible since only exergonic steps are included, while the M(0) cycle includes two slightly endergonic reactions. However, except of the first reaction, there are no big differences in the

Table 4. Amounts of ammonia and hydrogen after catalytic runs with SmI_2 and water.

Catalyst	NH_3 (equiv)	NH_3 (%)	H_2 (equiv)	H_2 (%)
[**Mo**(N_2)] (**1**)	25.73 ± 0.37[5]	43	52.02 ± 1.45	57
[**W**(N_2)] (**2**)	2.75 ± 0.23[10]	5	79.70 ± 3.81	89

Mo = Mo($P^{Me}_2PP^{Ph}_2$); **W** = W($P^{Me}_2PP^{Ph}_2$).

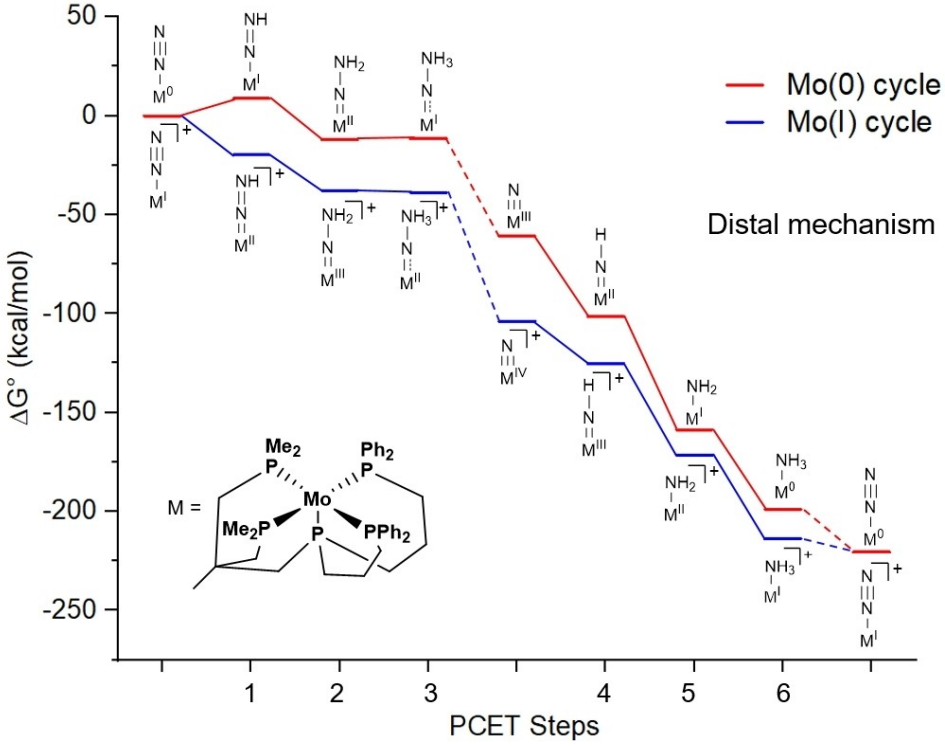

Figure 2. Energy scheme for the conversion of N_2 to NH_3 by PCET reactions starting from Mo(0)-N_2 (red) and $[Mo(I)\text{-}N_2]^+$ (blue) dinitrogen complexes. The dashed lines represent the NN cleavage. Since the energies of molybdenum and tungsten are very similar, only the energies of molybdenum are shown for clarity. For a complete energy diagram with tungsten, see Figure S1.

energetics of both cycles that would justify excluding one of them as possible reaction pathway. Notably, the tungsten complexes exhibit nearly the same energies as the molybdenum complexes, showing that the thermodynamics does not seem to be the reason for the different behavior under catalytic conditions (see Figure S1–S3).

To switch from the M(0) cycle to the M(I) cycle an intermediate of the M(I) cycle has to be generated. Starting from the M(0)-N_2 complex, possible candidates are the $[M(II)\text{-}NNH]^+$ and the $[M(III)\text{-}NNH_2]^+$ species. To generate these, the dinitrogen complex would have to be monoprotonated to obtain the $[M(II)\text{-}NNH]^+$ intermediate, which is part of the M(I) cycle, or diprotonated to generate the $[M(IV)\text{-}NNH_2]^{2+}$ species which then would have to be one-electron reduced. To this end, the SmI_2-water complex, or the corresponding Sm(III) species formed after PCET reaction, would have to be able to transfer electrons or protons individually besides acting as PCET reagent as assumed normally (Scheme 2).

As a second possibility, an alternating mechanism could be present (Figure 3, black). In the M(0) cycle, this pathway shows more exergonic steps for the first PCET reactions than the distal mechanism. While the first step to the M(0)(NHNH) species is only 5 kcal/mol more exergonic than the reaction to the M(II)(NNH_2) complex, the next step to the M(I)($NHNH_2$) complex, with about −30 kcal/mol, is highly exergonic compared to the slightly endergonic process (~ +0.5 kcal/mol) of the reaction to the M(I)(NNH_3) species. Additionally, formation of a M(0)($NHNH_3$)

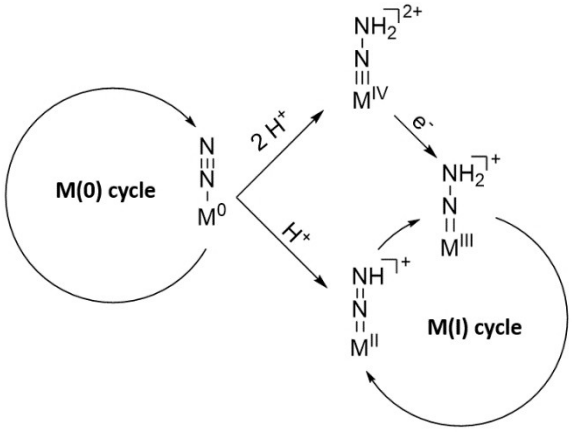

Scheme 2. Possible reaction pathways for switching from the M(0) cycle to the M(I) cycle by protonation of the M(0) dinitrogen complex (M = Mo, W) under catalytic conditions. Therefore, the SmI_2/H_2O mixture must react individually as acid and as reducing agent instead of PCET reagent.

intermediate (Figure 3, cyan) is principally possible. However, it is at higher energy than the other intermediates at this stage; that is, after 4 PCET steps, and therefore not likely to be formed.

Analogous results obtained for the M(I) cycle are shown in Figure 4. In contrast to the Mo(0) cycle, all PCET reactions correspond to exergonic steps. However, reaction of the $[M(II)(NNH)]^+$ to the $[M(I)(NHNH)]^+$ species is less exergonic than PCET to the distal nitrogen. The next step of the

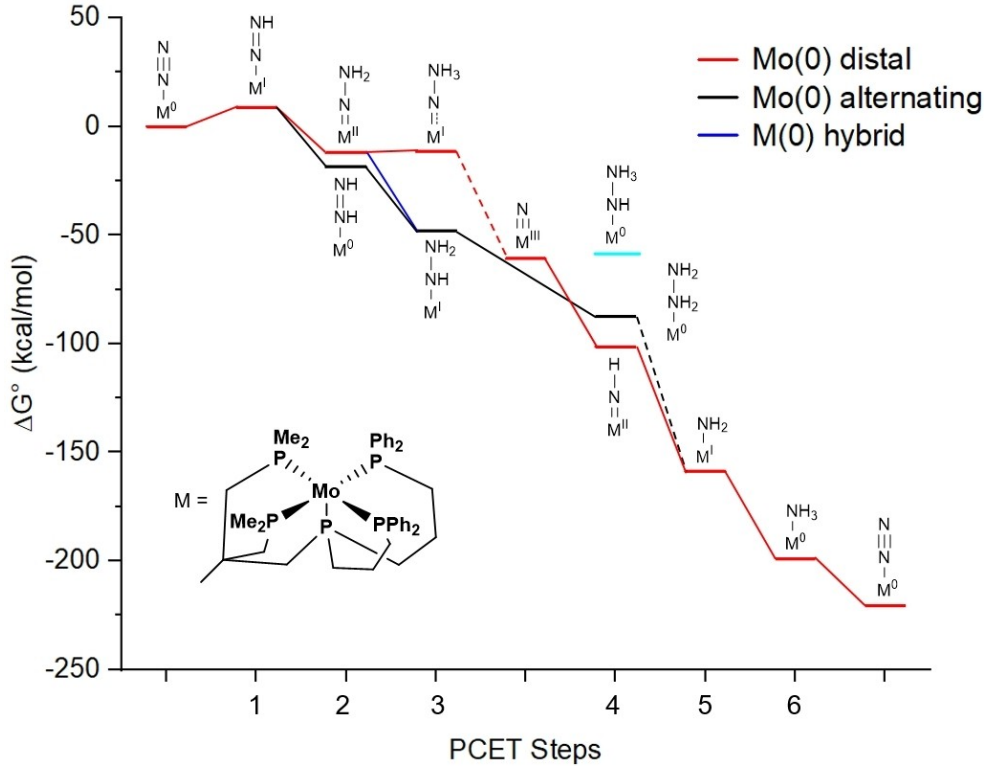

Figure 3. Energy scheme for the conversion of N_2 to NH_3 by PCET reactions of distal (red), alternating (black) and hybrid (blue) pathways starting from the Mo(0) dinitrogen complex. The dashed lines represent the NN cleavage. A mechanism by an alternating pathway shows exclusively exergonic steps compared to a distal pathway with two (slightly) endergonic steps. The $Mo(NH_2NH_3)$ species is not in this scheme because no geometry could be optimized without NN splitting and formation of NH_3. For a complete energy diagram with tungsten, see Figure S2. Cyan = high-energy intermediate.

alternating pathway, on the other hand, is highly exergonic compared to the PCET reaction to $[M(II)(NNH_3)]^+$, which is just a slightly exergonic process. The following steps do not differ significantly between distal and alternating modes. Finally, a hybrid mechanism where a $[M(II)(NHNH_2)]^+$ complex is formed through PCET to $[M(III)(NNH_2)]^+$ represents a more exergonic alternative to the formation of $[M(II)(NNH_3)]^+$. Again, a $[M(I)(NHNH_3)]^+$ intermediate could in principle form, but is at higher energy than other intermediates at this stage (Figure 4, cyan). To conclude, all three scenarios are feasible for the Mo(I) cycle, but it has to be kept in mind that the actual pathway also depends on kinetic factors. In this regard, PCET reactions on the distal nitrogen are generally preferred due to steric reasons.

HER Pathways

In the literature two main pathways for HER are discussed, namely bimolecular reactions of early M-N_xH_y intermediates (Scheme 3) and the formation of hydrogen via hydride species.[16,21,22] For our system we first identified the M-N_xH_y species that have a sufficiently low $BDFE_{N-H}$ to undergo a bimolecular reaction with release of hydrogen to an exergonic process.

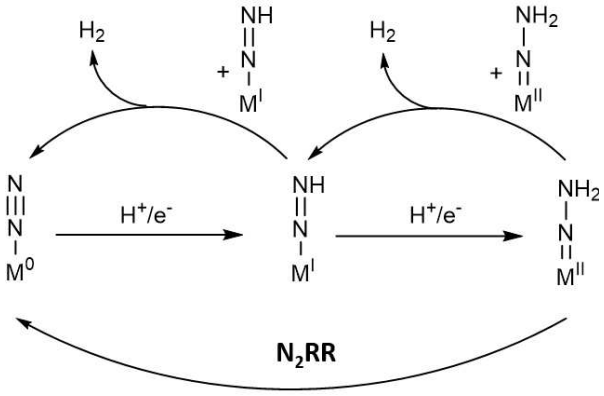

Scheme 3. Possible reaction pathways for the HER reaction from early M-N_xH_y intermediates of the M(0) cycle via bimolecular reaction (M = Mo, W), in concurrence to the N_2RR pathways.

a. Bimolecular reactions of early intermediates

Bimolecular reactions of early intermediates (cf. Scheme 4) are shown in Figure 5 for the Mo(0) and in Figure 6 for the Mo(I) cycle (green traces). In the former, they are in part more exergonic than reactions of N_2RR in Figure 5 (red, blue). In particular, bimolecular reactions of the M(I)-NNH intermediates show extremely exergonic ΔG values with −81.7 kcal/mol for

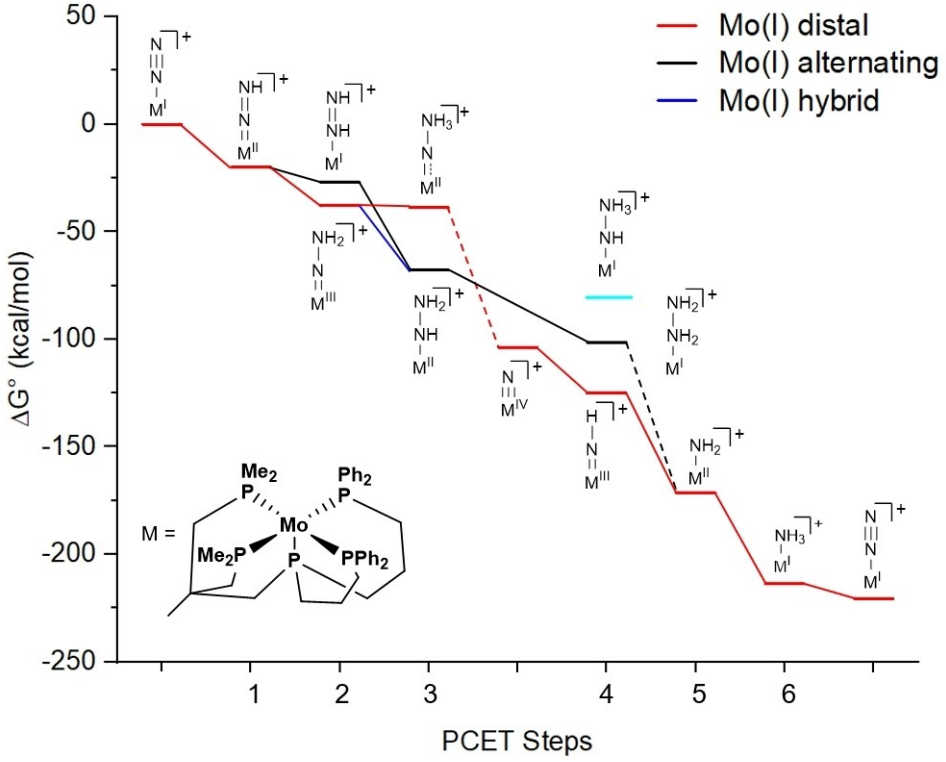

Figure 4. Energy scheme for the conversion of N_2 to NH_3 by PCET reactions of distal (red), alternating (black) and hybrid (blue) pathways starting from a Mo(I) dinitrogen complex. The dashed lines represent the NN cleavage The $Mo(NH_2NH_3)$ species is not in this scheme because no geometry could be optimized without NN splitting and formation of NH_3. For a complete energy diagram with tungsten, see Figure S3. Cyan = high-energy intermediate.

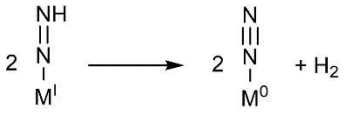

Scheme 4. Bimolecular reaction of [M(I)-NNH] leads to the formation of two equiv of the M(0)-N_2 complex and hydrogen (M = Mo, W).

molybdenum and −77.1 kcal/mol for tungsten (Figure S5), being much more negative than for PCET to the M(II)-NNH_2 intermediates (M = Mo, W; Table S12).

As pointed out by Benedek et al. for corresponding iron species,[21] the Mo(I)-NNH intermediate, for example, must have a sufficiently long lifetime for a bimolecular reaction to take place. Since a very high excess of PCET reagent is used under catalytic conditions, further reaction to the Mo(II)-NNH_2 intermediate, which is also a fairly exergonic process, is likely. PCET to Mo(II)-NNH_2 leading to M(I)-NNH_3 is slightly endergonic, and the former species thus could have a higher probability to undergo a bimolecular reaction. The same may apply to the Mo(I)-NNH_3 species due to its very low $BDFE_{N-H}$, but appears less probable in view of the fact that release of ammonia and formation of the nitride complex are highly exergonic. Moreover, the system may avoid the M(I)-NNH_3 intermediate by PCET to the proximal N, generating the lower-energy M(I)-$NHNH_2$ species (Figure 5, blue). Finally, PCET to the metal could lead to a mixed M(H)(NNH_2) intermediate that releases hydrogen in a monomolecular reaction (cf. Figure 5 black).

After the first equivalent of ammonia is released, bimolecular reactions of the (late) Mo-N_xH_y intermediates all show endergonic values in the M(0) cycle, which correlates with the calculated BDFEs (cf. Table 5). On the other hand, the PCET reactions in the second half of the M(0) cycle are highly exergonic, and thus bimolecular reactions can be excluded for the late Mo-N_xH_y intermediates of this cycle.

In the M(I) cycle, bimolecular reactions of early M-N_xH_y intermediates are less favored than in the M(0) cycle, as the competing steps of N_2RR are more feasible and should have a higher probability in the presence of an excess of PCET reagent (Figure 6). Analogous to the M(0) cycle bimolecular reaction of the $[M(II)\text{-}NNH]^+$ species is exergonic, but the difference to the PCET reaction forming the $[M(III)\text{-}NNH_2]^+$ species is small. Moreover, due to the large excess of PCET reagent, the bimolecular reaction is less likely than the further reaction to the hydrazido(2-) complex. In contrast, the bimolecular reaction starting from the $[M(III)\text{-}NNH_2]^+$ complex is significantly more exergonic than the PCET reaction leading to $[M(II)\text{-}NNH_3]^+$.

Again, formation of the $[M(II)\text{-}NHNH_2]^+$ intermediate is much more favorable and in fact the most exergonic possibility here. Moreover, this reaction should also be kinetically more feasible than the PCET reaction to a $[M(IV)(H)(NNH_2)]^+$ complex which may generate H_2 in a monomolecular reaction (cf. Figure 6, black).

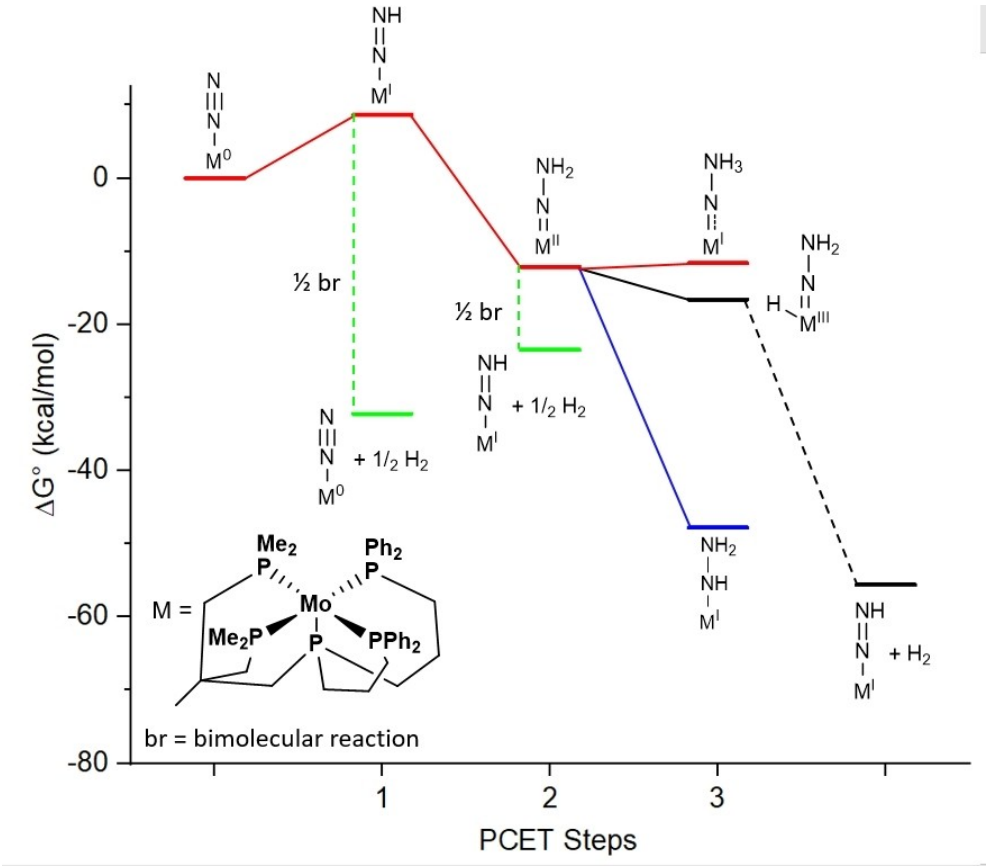

Figure 5. Energy scheme for HER via bimolecular reactions of early Mo-N_xH_y intermediates (green) compared to PCET reactions of the N_2RR pathway (distal red, hybrid blue) starting from the Mo(0)-N_2 complex. Additionally, HER via mixed M(H)(N_xH_y) intermediates is shown (black). Dashed lines represent the formation of hydrogen. For a complete energy diagram with tungsten, see Figure S4.

Table 5. Calculated $BDFE_{N–H}$ (terminal N–H bonds) of different M-N_xH_y species (x = 1-2, y = 1-4) of both possible catalytic cycles following distal and alternating pathways (for complete data, see Table S3–S5 in the Supporting Information).

Pathway	Complexes M(0) cycle	$BDFE_{N–H}$ [kcal/mol]		Complexes M(I) cycle	$BDFE_{N–H}$ [kcal/mol]	
		Mo	W		Mo	W
D + A	M(I)-NNH	17.3	19.6	$[M(II)\text{-}NNH]^+$	45.8	49.6
D	M(II)-NNH_2	46.8	47.9	$[M(III)\text{-}NNH_2]^+$	43.9	42.8
D	M(I)-NNH_3	25.5	25.5	$[M(II)\text{-}NNH_3]^+$	27.1	27.6
A	M(0)-NHNH	53.3	52.3	$[M(I)\text{-}NHNH]^+$	75.0	76.5
A	M(I)-$NHNH_2$	55.2	56.0	$[M(II)\text{-}NHNH_2]^+$	67.0	68.9
–	M(0)-$NHNH_3$	38.7	37.0	$[M(I)\text{-}NHNH_3]^+$	38.2	38.3
A	M(0)-NH_2NH_2	65.8	62.5	$[M(I)\text{-}NH_2NH_2]^+$	59.3	54.5
D + A	M(II)-NH	66.7	64.9	$[M(III)\text{-}NH]^+$	47.3	47.8
D + A	M(I)-NH_2	83.2	79.8	$[M(II)\text{-}NH_2]^+$	72.3	72.1
D + A	M(0)-NH_3	66.4	63.9	$[M(I)\text{-}NH_3]^+$	68.4	61.9

M = Mo($P^{Me}{}_2PP^{Ph}{}_2$), W($P^{Me}{}_2PP^{Ph}{}_2$), D = distal, A = alternating.

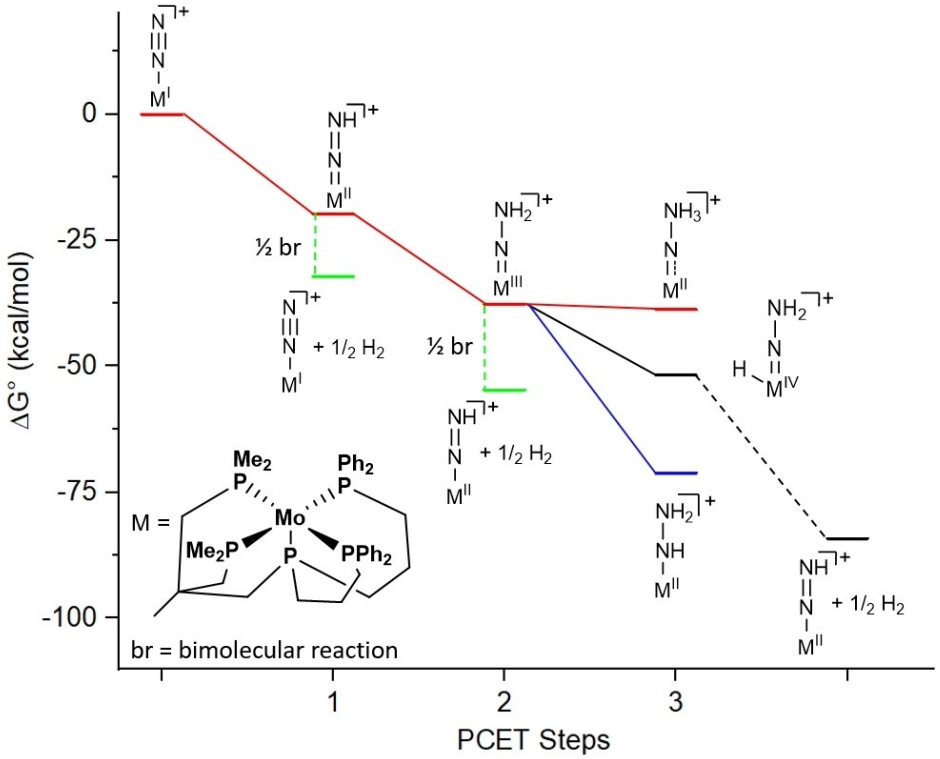

Figure 6. Energy scheme for HER via bimolecular reactions of early Mo-N_xH_y intermediates (green) compared to PCET reactions of the N_2RR pathway (distal red, hybrid blue) starting from the $[Mo(I)\text{-}N_2]^+$ complex. Additionally, HER via mixed $M(H)(N_xH_y)$ intermediates is shown (black). Dashed lines represent the formation of hydrogen. For a complete energy diagram with tungsten, see Figure S5.

b. Hydride pathway

The second possibility, HER via hydride species, is shown in Figure 7 for the M(0) and in Figure 8 for the M(I) cycle (red traces). In the former, it starts from a neutral M(I)-H complex. For the generation of this species two pathways are possible (Figure 7, red): either the N_2-ligand dissociates before PCET occurs or PCET takes place first under formation of a $M(I)(H)(N_2)$ intermediate, and then the N_2-ligand decoordinates. Dissociation of the N_2-ligand under formation of a M(0) complex with a free coordination site is a strongly endergonic process with +29.4 kcal/mol for W and +24.6 kcal/mol for Mo. Although the following PCET is highly exergonic (−43.4 kcal/mol for W and −37.0 kcal/mol for Mo) the barrier of the N_2-decoordination seems too high to follow this pathway. When PCET takes place first, forming a $M(I)(H)(N_2)$ species, it is just a slightly endergonic process comparable with the generation of the M(I)-NNH intermediate. The subsequent decoordination of the dinitrogen ligand is strongly exergonic (−20.7 kcal/mol for W and Mo). In the presence of an excess of PCET reagent the M(I)-H complex should be further converted into a $M(II)\text{-}(H)_2$ species in a highly exergonic process (−40.6 kcal/mol for W and −40.0 kcal/mol for Mo). Based on this dihydride complex the release of hydrogen in a reductive elimination under formation of a M(0) complex with a free coordination site is an endergonic process with ΔG-values above +10 kcal/mol. For tungsten, the value is about 7 kcal/mol larger than for molybdenum. HER by this "hydride pathway" thus should be more feasible for molybdenum than for tungsten whence it cannot explain the difference in HER behavior between these two metals. When calculating the free Gibbs energy of the hydrogen release in the presence of dinitrogen; that is, under formation of a M(0) dinitrogen complex, this process is exergonic with values about −10 kcal/mol. If reductive elimination is not possible for the release of hydrogen from a $M(II)\text{-}(H)_2$ complex, an associative mechanism via 8-coordinate $M(II)(H)_2(N_2)$ transition state under a dinitrogen atmosphere might be another option. This intermediate, however, could not be optimized and probably also involves large kinetic barriers for its formation and decay.

Besides pure hydride complexes, a combination of early M-N_xH_y intermediates and hydride should not be neglected and could be more feasible regarding HER for the more electron-rich tungsten complexes (Figures 8 and 9, black traces).[9] In addition, the hydrogen atoms here would already be polarized with a partially positively charged N–H hydrogen and a partially negatively charged hydride. For the M(0) cycle, formation of a M(II)(H)(NNH) species by PCET to M(I)-NNH or $M(I)(N_2)(H)$ is slightly endergonic (~ +7 kcal/mol for W and +5 kcal/mol for Mo), with a huge exergonic process (< −60 kcal/mol) for the following hydrogen release under formation of the M(0)-N_2 complex (see Figure 7, black). A similar pathway based on the $M(II)\text{-}NNH_2$ species to a $M(III)(H)(NNH_2)$ intermediate and evolution of hydrogen under formation of the Mo(I)-NNH

Table 6. Gibbs free energies (ΔG) and Gibbs free activation energies ($\Delta G^{\ddagger}$) for bimolecular HER of early M-N_xH_y intermediates compared to competing N_2RR steps and PCET at the metal center in kcal/mol.

Reaction type	M(I)-NNH				M(II)-NNH_2			
M(0) cycle	Mo		W		Mo		W	
	$BDFE_{N-H}=17.3$		$BDFE_{N-H}=19.6$		$BDFE_{N-H}=46.8$		$BDFE_{N-H}=47.9$	
	ΔG	$\Delta G^{\ddagger}$ [a]	ΔG	$\Delta G^{\ddagger}$ [a]	ΔG	$\Delta G^{\ddagger}$ [a]	ΔG	$\Delta G^{\ddagger}$ [a]
Bimolecular HER	−40.8	0.6	−38.6	1.6	-11.4	13.7	-10.3	10.2
$\Delta G_R(SmI_2/H_2O)$ for PCET to distal N	−20.8	–	−21.9	–	+0.5	-	+0.5	-
$\Delta G_R(SmI_2/H_2O)$ f. PCET to prox. N	−27.3	–	−26.3	–	-35.7	-	-34.5	-
$\Delta G_R(SmI_2/H_2O)$ f. PCET to met. cent.	−5.2	–	−7.0	–	-4.5	-	-7.2	-
Reaction type	$[M(II)-NNH]^+$				$[M(III)-NNH_2]^+$			
M(I) cycle	Mo		W		Mo		W	
	$BDFE_{N-H}=45.8$		$BDFE_{N-H}=49.6$		$BDFE_{N-H}=43.9$		$BDFE_{N-H}=42.8$	
	ΔG	$\Delta G^{\ddagger}$	ΔG	$\Delta G^{\ddagger}$	ΔG	$\Delta G^{\ddagger}$	ΔG	$\Delta G^{\ddagger}$
Bimolecular HER	−12.3	28.1	−8.5	27.8	-14.3	9.7	-15.4	9.2
$\Delta G_R(SmI_2/H_2O)$ for PCET to distal N	−17.9	–	−16.8	–	-1.1	-	-1.6	-
$\Delta G_R(SmI_2/H_2O)$ f. PCET to prox. N	−7.0	–	−4.7	–	-30.1	-	-30.8	-
$\Delta G_R(SmI_2/H_2O)$ f. PCET to met. cent.	+0.5	–	−0.1	–	-14.1	-	-17.7	-

M = Mo($P^{Me}{}_2PP^{Ph}{}_2$), W($P^{Me}{}_2PP^{Ph}{}_2$), [a] Gibbs free activation energies were calculated based on a truncated ligand system.

complex is also possible and exergonic, albeit a little less than for the M(II)(H)(NNH) species (Figure 5, black; see above).

For the M(I) cycle, pathways for HER via hydride species start from a cationic $[M(II)-H]^+$ species (Figure 8, red). The formation of this species over a dissociative mechanism, where the dinitrogen ligand of the $[M(I)-N_2]^+$ complex decoordinates before the PCET reaction on the metal center takes place, is unlikely due to the strongly endergonic N_2-dissociation step. An associative mechanism, on the other hand, in which a $[Mo(II)(H)(N_2)]^+$ complex is formed first, is highly exergonic. The subsequent decoordination of the N_2-ligand, however, would be endergonic (14.1 kcal/mol for W and +16.2 kcal/mol for Mo). A PCET reaction to $[Mo(III)(H)(NNH)]^+$ shows similar energetics, but could cause release of hydrogen in a strongly exergonic way (cf. Figure 8, black). Alternatively, formation of a Mo(III) dihydride complex from the monohydride species is also strongly exergonic with -38.6 kcal/mol for tungsten and −35.7 kcal/mol for molybdenum. Hydrogen release from the $[Mo(III)-(H)_2]^+$ complex would be a significantly less endergonic reaction compared to the Mo(II)-$(H)_2$ species of just +8.2 kcal/mol for molybdenum and +17.5 kcal/mol for tungsten. However, since this would mean that molybdenum should have a higher activity with respect to the HER, this would not provide an explanation for the different reactivity of these two metals in **1** and **2**.

If the reactions are considered with regard to their kinetics, it can be assumed that the formation of the early M-N_xH_y intermediates probably involves lower activation barriers than PCET reactions directly at the metal center due to the sterically shielding ligand system. This is supported by the experimental finding that the $[M(IV)-NNH_2]^{2+}$ complexes can be obtained through protonation with $HBAr^F$ ($[H(OEt_2)_2][BAr^F]$, BAr^F = tetrakis(3,5-bis(trifluoro-methyl)phenyl)borate),[5] although direct protonation at the metal center to give a $[M(II)(N_2)(H)]^+$ species would be favored thermodynamically (free Gibbs energy of <-35.0 kcal/mol compared to about −20.0 kcal/mol for the first protonation to a diazenido intermediate ($[M(II)-NNH]^+$). On the other hand, the $[M(II)-NNH]^+$ species could not be isolated by protonation with one equivalent of acid, reflecting a low stability of this intermediate. This may be due to the fact that the bimolecular reaction of the $[M(II)-NNH]^+$ complex leading to the $[M(I)-N_2]^+$ complex and H_2 is exergonic (−17.0 kcal/mol for W and −24.7 kcal/mol for Mo; Figure 6, green). In contrast, for the $[M(IV)-NNH_2]^{2+}$ complexes which can be generated through protonation, the bimolecular reaction is strongly endergonic ($\Delta G > 25$ kcal/mol), leading to a much higher stability of the hydrazido(2-) complexes of tungsten and molybdenum. However, an excess (2.5 to 3 equiv) of acid is needed for the synthesis of the $[M(IV)-NNH_2]^+$ complexes,[5,10] to speed up the reaction and lower the lifetime of the $[M(II)-NNH]^+$ species which otherwise is accessible for bimolecular reactions and thus for hydrogen formation.

Table 7. Gibbs free energies (ΔG) and activation Gibbs free energy ($\Delta G^{\ddagger}$) and $BDFE_{N-H}$ in kcal/mol for HER based on mixed $M(H)(N_xH_y)$ (M = Mo, W) intermediates.

M(II)(H)(NNH)				[M(III)(H)(NNH)]$^+$				[M(IV)(H)(NNH_2)]$^+$			
Mo		W		Mo		W		Mo		W	
ΔG	ΔG‡	ΔG	ΔG‡	ΔG	ΔG‡	ΔG	ΔG‡	ΔG	ΔG‡	ΔG	ΔG‡
−67.8	6.2	−63.8	5.8	−45.0	26.4	−40.6	26.5	−32.3	22.2	−29.8	19.4

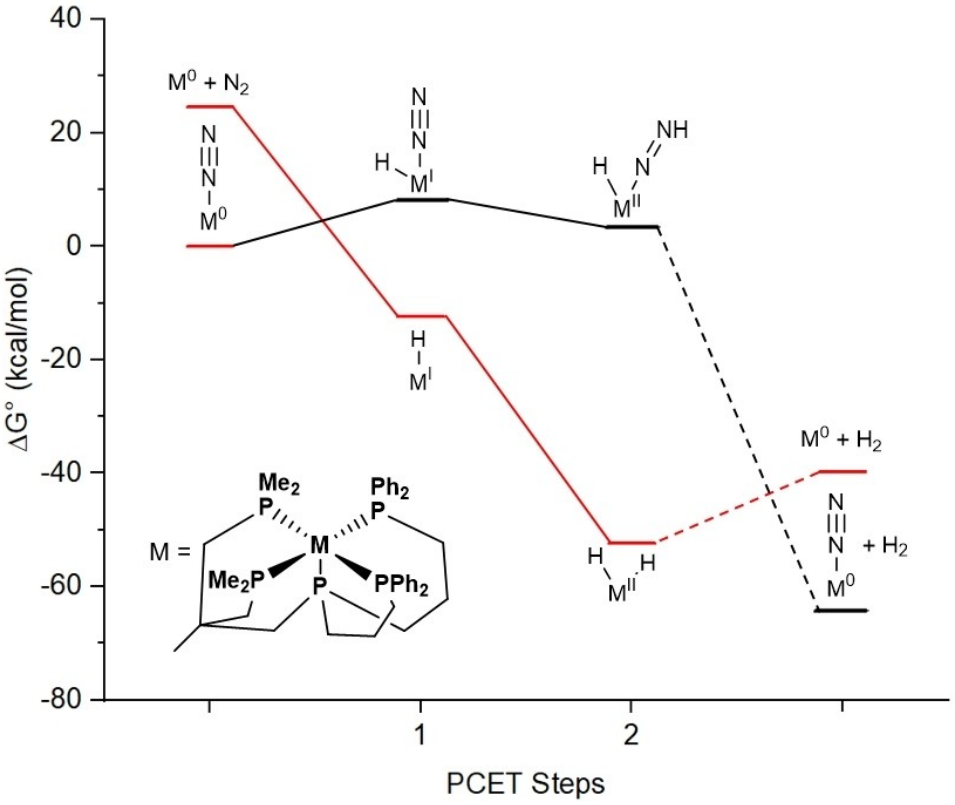

Figure 7. Energy scheme for some possible intramolecular HER involving metal hydride species starting from Mo(0)-N_2 complex (red: HER via pure hydride species, black: HER via M(H)(NNH). Dashed lines represent the formation of hydrogen. For a complete energy diagram with tungsten, see Figure S6.

Calculation of kinetic barriers for HER

In order to predict the most likely mechanism for HER, consideration of only BDFE's and the thermodynamics of PCET processes is not sufficient. Therefore, activation barriers were calculated for bimolecular reactions on the one hand (Table 6) and for the formation of hydrogen from mixed $M(H)(N_xH_y)$ species on the other hand (Table 7). As the large pentaPod ligand requires long computation times, the equatorial phosphine groups were truncated to PH_2 groups for the calculation of bimolecular transition states. Although the steric properties of the ligand get lost this way, a comparison of activation barriers should provide insight into differences between neutral and cationic intermediates as well as between Mo and W.

Importantly, activation barriers for the bimolecular reactions are significantly lower for the M-NNH intermediate of the M(0) cycle than for the M(I) cycle. While for the M(I)-NNH intermediate just a small activation barrier via a bimolecular transition state (Figure 9A) is present, for the M(II)-NNH_2 intermediate activation barriers of 13.7 kcal/mol (Mo) and 10.2 kcal/mol (W) apply. In contrast, the respective M-NNH intermediate of the M(I) cycle shows an activation barrier which is more than 25 kcal/mol higher than for the M(0) cycle intermediate, while the M-NNH_2 intermediates show comparable activation barriers in both cycles. HER via a bimolecular mechanism thus should primarily occur in the M(0) cycle at the M-NNH stage, whereas HER from early intermediates of the M(I) cycle is less probable.

Similar trends are observed for HER via mixed $M(H)(N_xH_y)$ intermediates, where [M(III)(H)(NNH)]$^+$ and [M(IV)(H)(NNH_2)]$^+$ complexes show activation barriers between 19.4 and 26.5 kcal/mol whereas for neutral M(II)(H)(NNH) complexes activation barriers of only 5.8 kcal/mol for W and 6.2 kcal/mol for Mo apply (Table 7). Moreover, HER from neutral intermediates is also more exergonic compared to that from monocationic ones. The transition state for HER from the Mo(II)(H)(NNH) intermediate involves a 5-membered N_2H_2-metallacycle (Figure 9B). For the

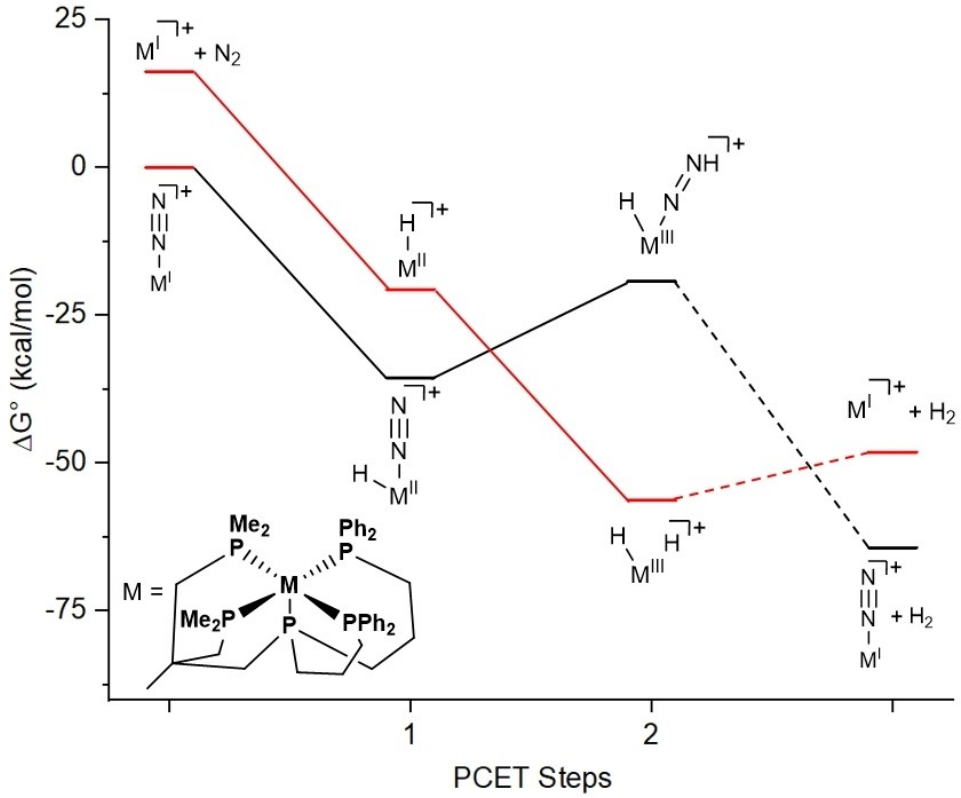

Figure 8. Energy scheme for some possible intramolecular HER involving metal hydride species starting from Mo(I)-N_2 complex (red: HER via pure hydride species, black: HER via $[M(H)(NNH)]^+$ For a complete energy diagram with tungsten, see Figure S7.

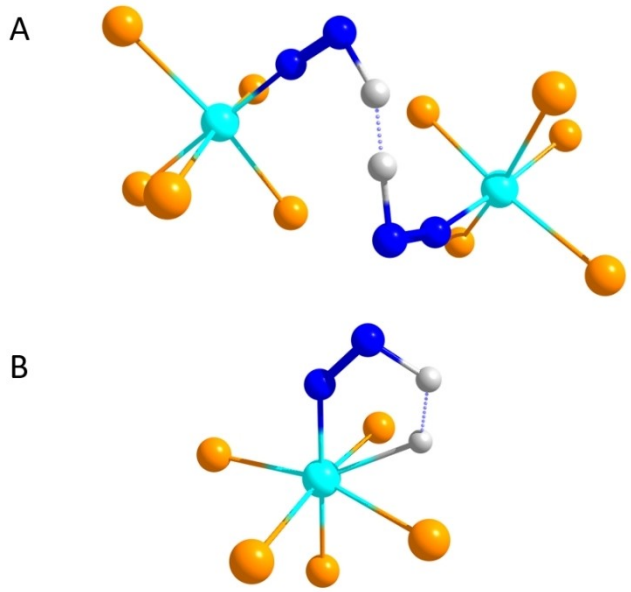

Figure 9. Optimized structures of transitions states of $[Mo(NNH)P_5]_2$ (A) and [Mo(H)(NNH)(pentaPod)] (B) (molybdenum = light blue, phosphorus = orange, nitrogen = blue and hydrogen = white, P_5 = truncated pentaPod ligand).

M(III)(H)(NNH_2) intermediate no transition state for the evolution of hydrogen could be found. Compared to PCET reactions at the distal or proximal nitrogen, PCET directly to the metal center should be kinetically disfavored and thus may prevent the formation of a hydride species (see above).

Notably, molybdenum and tungsten show no significant difference in activation barriers (maximum 3.5 kcal/mol, cf Table 6), so that the results obtained for the kinetics of HER in this section do not provide an explanation for the different reaction behavior under turnover conditions. A possible reason could be the kinetics of PCET being different for the Mo and W systems. A theoretical treatment of this problem is outside the scope of the present study.

Conclusion

We showed at the beginning that the tungsten dinitrogen complex with a pentadentate tetrapodal phosphine ligand exhibits a higher HER and a lower N_2RR activity than its molybdenum analogue. This led us to the question of the reason for these different reactivities, which was studied theoretically using DFT calculations. For this purpose, we first investigated the most probable mechanism of catalytic N_2-to-NH_3 conversion mediated by Mo- and W-pentaPod complexes. It was found that the thermodynamically most favorable pathways depend on whether the starting dinitrogen complex is neutral (→M(0) cycle) or cationic (→M(I) cycle). For the M(0) cycle an alternating pathway seems to be preferred, due to

exclusively exergonic steps except for an endergonic step for the first PCET reaction. For the M(I) cycle, in contrast, a hybrid mechanism via a M(II)($NHNH_2$) complex shows the most exergonic pathway compared to a strictly distal or an alternating mechanism. To switch from the M(0) cycle to the M(I) cycle the PCET reagent (SmI_2/H_2O) must be able to protonate the M(0)-N_2 complex without electron transfer or reduce the [M(IV)-(NNH_2)]$^{2+}$ complex without proton transfer.

After treatment of N_2RR, possible mechanisms of HER were determined, and their thermodynamics and kinetics were investigated. Three possible pathways were treated theoretically, based on hydrogen generation through 1) bimolecular reactions of early M-N_xH_y intermediates; 2) hydride complexes; and (3) mixed M(H)(N_xH_y) complexes. Calculations of bimolecular pathways indicate that, among the early intermediates of the M(0) cycle, the neutral M(I)(NNH) complexes of molybdenum and tungsten have the lowest BDFEs, show the most exergonic reactions and exhibit the lowest activation barriers. Early intermediates of the M(I) cycle, on the other hand, show higher activation barriers for bimolecular reactions and exhibit less exergonic reactions in the generation of hydrogen, so that these less likely promote HER.

Hydrogen evolution via hydride complexes always involves endergonic reactions, which are thermodynamically less favorable than other pathways. Additionally, PCET reactions directly at the metal center should be kinetically disfavored in comparison to PCET reactions at the distal or proximal nitrogen, due to steric reasons. HER via mixed M(H)(N_xH_y) species, in contrast, is highly exergonic, again showing lower activation barriers for neutral than for monocationic intermediates. This further indicates that HER is more likely when starting from intermediates of the M(0) cycle.

In summary, the results of this study lead to the following conclusions:

- To minimize HER and maximize N_2RR, experimental conditions should be chosen such as to avoid the M(0) cycle. This can be achieved by preventing "over-reduction" through PCET reagents with a suitable redox potential.
- Bimolecular reactions and H-transfer to the metal center should be suppressed as far as possible. This can be effected by introducing sterically more demanding phosphines than PMe_2 groups (e.g., phospholane or diisopropylphosphine groups).
- Regarding the thermodynamics of N_2RR and the thermodynamics/kinetics of hydrogen evolution from hydride or mixed NNH_x/hydride intermediates, the calculations suggest that no significant differences between molybdenum and tungsten exist.
- Differences in reactivity between Mo and W systems thus may be due to kinetic barriers of PCET along the N_2RR pathway, on which we have not obtained theoretical information in this study. Notably, tungsten complexes require longer reaction times in catalytic experiments (days) than molybdenum complexes (hours; cf. Table S22). This could be due to higher kinetic barriers for PCET reactions, leading to slower conversion of intermediates along the N_2RR pathway. Thus, bimolecular reactions become more likely (or even dominant) for the tungsten systems, in contrast to the molybdenum analogues, in which the corresponding intermediates are more rapidly converted towards N_2RR.

Slower PCET to the tungsten complexes in comparison with their molybdenum analogues may be caused by lower (more negative) reduction potentials, increasing the barriers for these processes.[43] In any case, understanding the factors, which determine the kinetics of PCET in Mo- vs. W-based N_2RR-catalysts, will require further experimental and theoretical work.

Acknowledgements

The authors thank B. Mockenhaupt for the assistance during the GC measurements and the CAU Kiel for the financial support. Open Access funding enabled and organized by Projekt DEAL.

Conflict of Interest

The authors declare no conflict of interest.

Data Availability Statement

The data that support the findings of this study are available in the supplementary material of this article.

Keywords: molybdenum · nitrogen fixation · reaction mechanisms · tungsten

[1] a) J. S. Anderson, J. Rittle, J. C. Peters, *Nature* **2013**, *501*, 84; b) J. Chatt, A. J. Pearman, R. L. Richards, *Nature* **1975**, *253*, 39; c) M. J. Chalkley, M. W. Drover, J. C. Peters, *Chem. Rev.* **2020**, *120*, 5582; d) Y. Tanabe, Y. Nishibayashi, *Chem. Soc. Rev.* **2021**, *50*, 5201; e) N. Stucke, B. M. Flöser, T. Weyrich, F. Tuczek, *Eur. J. Inorg. Chem.* **2018**, *2018*, 1337.
[2] D. V. Yandulov, R. R. Schrock, *Science* **2003**, *301*, 71.
[3] K. Arashiba, Y. Miyake, Y. Nishibayashi, *Nat. Chem.* **2011**, *3*, 120.
[4] a) T. J. Del Castillo, N. B. Thompson, J. C. Peters, *J. Am. Chem. Soc.* **2016**, *138*, 5341; b) A. Eizawa, K. Arashiba, H. Tanaka, S. Kuriyama, Y. Matsuo, K. Nakajima, K. Yoshizawa, Y. Nishibayashi, *Nat. Commun.* **2017**, *8*, 14874.
[5] T. A. Engesser, A. Kindjajev, J. Junge, J. Krahmer, F. Tuczek, *Chem. Eur. J.* **2020**, *26*, 14807.
[6] Y. Ashida, K. Arashiba, K. Nakajima, Y. Nishibayashi, *Nature* **2019**, *568*, 536.
[7] a) H. Tanaka, K. Arashiba, S. Kuriyama, A. Sasada, K. Nakajima, K. Yoshizawa, Y. Nishibayashi, *Nat. Commun.* **2014**, *5*, 3737; b) S. Kuriyama, K. Arashiba, K. Nakajima, H. Tanaka, N. Kamaru, K. Yoshizawa, Y. Nishibayashi, *J. Am. Chem. Soc.* **2014**, *136*, 9719; c) K. Arashiba, E. Kinoshita, S. Kuriyama, A. Eizawa, K. Nakajima, H. Tanaka, K. Yoshizawa, Y. Nishibayashi, *J. Am. Chem. Soc.* **2015**, *137*, 5666; d) Y. Ashida, K. Arashiba, H. Tanaka, A. Egi, K. Nakajima, K. Yoshizawa, Y. Nishibayashi, *Inorg. Chem.* **2019**, *58*, 8927.
[8] R. R. Schrock, *Acc. Chem. Res.* **2005**, *38*, 955.
[9] K. Arashiba, K. Sasaki, S. Kuriyama, Y. Miyake, H. Nakanishi, Y. Nishibayashi, *Organometallics* **2012**, *31*, 2035.
[10] J. Junge, S. Froitzheim, T. A. Engesser, J. Krahmer, C. Näther, N. Le Poul, F. Tuczek, *Dalton Trans.* **2022**, 6166.
[11] D. V. Yandulov, R. R. Schrock, *Can. J. Chem.* **2005**, *83*, 341.
[12] a) A. Döring, C. Schulzke, *Dalton Trans.* **2010**, *39*, 5623; b) U. Ryde, C. Schulzke, K. Starke, *J. Biol. Inorg. Chem.* **2009**, *14*, 1053; c) C. Schulzke, *Dalton Trans.* **2005**, 713.

[13] S. Hinrichsen, A. Kindjajev, S. Adomeit, J. Krahmer, C. Näther, F. Tuczek, *Inorg. Chem.* **2016**, *55*, 8712.
[14] J. Junge, T. A. Engesser, J. Krahmer, C. Näther, F. Tuczek, *Z. Anorg. Allg. Chem.* **2021**, *647*, 822.
[15] a) L. C. Seefeldt, B. M. Hoffman, D. R. Dean, *Annu. Rev. Biochem.* **2009**, *78*, 701; b) B. M. Hoffman, D. Lukoyanov, Z.-Y. Yang, D. R. Dean, L. C. Seefeldt, *Chem. Rev.* **2014**, *114*, 4041; c) S. Simpson, F. B. Burris, *Science* **1984**, *224*, 1095; d) J. B. Varley, Y. Wang, K. Chan, F. Studt, J. K. Nørskov, *Phys. Chem. Chem. Phys.* **2015**, *17*, 29541.
[16] B. D. Matson, J. C. Peters, *ACS Catal.* **2018**, *8*, 1448.
[17] a) S. Kuriyama, K. Arashiba, K. Nakajima, H. Tanaka, N. Kamaru, K. Yoshizawa, Y. Nishibayashi, *J. Am. Chem. Soc.* **2014**, *136*, 9719; b) B. Schluschaß, J. Abbenseth, S. Demeshko, M. Finger, A. Franke, C. Herwig, C. Würtele, I. Ivanovic-Burmazovic, C. Limberg, J. Telser et al., *Chem. Sci.* **2019**, *10*, 10275.
[18] D. J. Schild, J. C. Peters, *ACS Catal.* **2019**, *9*, 4286.
[19] J. Fajardo, J. C. Peters, *Inorg. Chem.* **2021**, *60*, 1220.
[20] M. J. Chalkley, J. C. Peters, *Eur. J. Inorg. Chem.* **2020**, *2020*, 1353.
[21] Z. Benedek, M. Papp, J. Oláh, T. Szilvási, *Inorg. Chem.* **2019**, *58*, 7969.
[22] Z. Benedek, M. Papp, J. Oláh, T. Szilvási, *Inorg. Chem.* **2018**, *57*, 8499.
[23] F. Neese, *WIREs Comput. Mol. Sci.* **2018**, *8*, 33.
[24] J. P. Perdew, K. Burke, M. Ernzerhof, *Phys. Rev. Lett.* **1996**, *77*, 3865–3686.
[25] A. Schäfer, H. Horn, R. Ahlrichs, *J. Chem. Phys.* **1992**, *97*, 2571.
[26] A. Schäfer, C. Huber, R. Ahlrichs, *J. Chem. Phys.* **1994**, *100*, 5829.
[27] F. Weigend, R. Ahlrichs, *Phys. Chem. Chem. Phys.* **2005**, *7*, 3297.
[28] S. Grimme, J. Antony, S. Ehrlich, H. Krieg, *J. Chem. Phys.* **2010**, *132*, 154104.
[29] S. Grimme, S. Ehrlich, L. Goerigk, *J. Comput. Chem.* **2011**, *32*, 1456.
[30] K. Eichkorn, O. Treutler, H. Öhm, M. Häser, R. Ahlrichs, *Chem. Phys. Lett.* **1995**, *240*, 283.
[31] K. Eichkorn, F. Weigend, O. Treutler, R. Ahlrichs, *Theor. Chem. Acc.* **1997**, *97*, 119.
[32] F. Neese, *J. Comput. Chem.* **2003**, *24*, 1740.
[33] F. Neese, F. Wennmohs, A. Hansen, U. Becker, *Chem. Phys.* **2009**, *356*, 98.
[34] C. van Wüllen, *J. Chem. Phys.* **1998**, *109*, 392.
[35] a) J. D. Rolfes, F. Neese, D. A. Pantazis, *J. Comput. Chem.* **2020**, *41*, 1842; b) M. Bühl, C. Reimann, D. A. Pantazis, T. Bredow, F. Neese, *J. Chem. Theory Comput.* **2008**, *4*, 1449; c) D. A. Pantazis, X.-Y. Chen, C. R. Landis, F. Neese, *J. Chem. Theory Comput.* **2008**, *4*, 908.
[36] C. Kollmar, *Int. J. Quantum Chem.* **1997**, *62*, 617.
[37] a) A. D. Becke, *Phys. Rev. A* **1988**, *38*, 3098; b) J. P. Perdew, *Phys. Rev. B* **1986**, *33*, 8822.
[38] R. Poli, J. N. Harvey, *Chem. Soc. Rev.* **2003**, *32*, 1.
[39] J. N. Harvey, *Phys. Chem. Chem. Phys.* **2007**, *9*, 331.
[40] A. V. Marenich, C. J. Cramer, D. G. Truhlar, *J. Phys. Chem. B* **2009**, *113*, 6378.
[41] C. F. Wise, R. G. Agarwal, J. M. Mayer, *J. Am. Chem. Soc.* **2020**, *142*, 10681.
[42] S. S. Kolmar, J. M. Mayer, *J. Am. Chem. Soc.* **2017**, *139*, 10687.
[43] R. Tyburski, T. Liu, S. D. Glover, L. Hammarström, *J. Am. Chem. Soc.* **2021**, *143*, 560.

Manuscript received: August 23, 2022
Accepted manuscript online: December 2, 2022
Version of record online: January 27, 2023